Numerical solution of shock and ramp compression
for general material properties

Damian C. Swift[*]

Materials Science and Technilogy Division,

Lawrence Livermore National Laboratory,

7000, East Avenue, Livermore, CA 94550, U.S.A.

(Dated: March 7, 2007; revised April 8, 2008 – LA-UR-07-2051)

Abstract

A general formulation was developed to represent material models for applications in dynamic loading. Numerical methods were devised to calculate response to shock and ramp compression, and ramp decompression, generalizing previous solutions for scalar equations of state. The numerical methods were found to be flexible and robust, and matched analytic results to a high accuracy. The basic ramp and shock solution methods were coupled to solve for composite deformation paths, such as shock-induced impacts, and shock interactions with a planar interface between different materials. These calculations capture much of the physics of typical material dynamics experiments, without requiring spatially-resolving simulations. Example calculations were made of loading histories in metals, illustrating the effects of plastic work on the temperatures induced in quasi-isentropic and shock-release experiments, and the effect of a phase transition.

---

[*]Electronic address: damian.swift@physics.org

I. INTRODUCTION

The continuum representation of matter is widely used for material dynamics in science and engineering. Spatially-resolved continuum dynamics simulations are the most widespread and familiar, solving the initial value problem by discretizing the spatial domain and integrating the dynamical equations forward in time to predict the motion and deformation of components of the system. This type of simulation is used, for instance, to study hypervelocity impact problems such as the vulnerability of armor to projectiles [1, 2], the performance of satellite debris shields [3], and the impact of meteorites with planets, notably the formation of the moon [4]. The problem can be divided into the dynamical equations of the continuum, the state field of the components $s(\vec{r})$, and the inherent properties of the materials. Given the local material state s, the material properties allow the stress τ to be determined. Given the stress field $\tau(\vec{r})$ and mass density field $\rho(\vec{r})$, the dynamical equations describe the fields of acceleration, compression, and thermodynamic work done on the materials.

The equations of continuum dynamics describe the behavior of a dynamically deforming system of arbitrary complexity. Particular, simpler deformation paths can be described more compactly by different sets of equations, and solved by different techniques than those used for continuum dynamics in general. Simpler deformation paths occur often in experiments designed to develop and calibrate models of material properties. These paths can be regarded as different ways of interrogating the material properties. The principal examples in material dynamics are shock and ramp compression [5, 6]. Typical experiments are designed to induce such loading histories and measure or infer the properties of the material in these states before they are destroyed by release from the edges or by reflected waves.

The development of the field of material dynamics was driven by applications in the physics of hypervelocity impact and high explosive systems, including nuclear weapons [7]. In the regimes of interest, typically components with dimensions ranging from millimeters to meters and pressures from $1\,\mathrm{GPa}$ to $1\,\mathrm{TPa}$, material behavior is dominated by the scalar equation of state (EOS): the relationship between pressure, compression (or mass density), and internal energy. Other components of stress (specifically shear stresses) are much smaller, and chemical explosives react promptly so can be treated by simple models of complete detonation. EOS were developed as fits to experimental data, particularly

2

to series of shock states and to isothermal compression measurements [8]. It is relatively straightforward to construct shock and ramp compression states from an EOS algebraically or numerically depending on the EOS, and to fit an EOS to these measurements. More recently, applications and scientific interest have grown to include a wider range of pressures and time scales, such as laser-driven inertial confinement fusion [9], and experiments are designed to measure other aspects than the EOS, such as the kinetics of phase changes, constitutive behavior describing shear stresses, incomplete chemical reactions, and the effects of microstructure, including grain orientation and porosity. Theoretical techniques have also evolved to predict the EOS with ~1% accuracy [10] and elastic contributions to shear stress with slightly poorer accuracy [11].

In this paper, a general convention for representing material states is described, and numerical methods are reported for calculating shock and ramp compression states from general representations of material properties.

II. CONCEPTUAL STRUCTURE FOR MATERIAL PROPERTIES

The desired structure for the description of the material state and properties under dynamic loading was developed to be as general as possible with respect to the types of material or models to be represented in the same framework, and designed to give the greatest amount of commonality between spatially-resolved simulations and calculations of shock and ramp compressions.

In condensed matter on sub-microsecond time scales, heat conduction is often too slow to have a significant effect on the response of the material, and is ignored here. The equations of non-relativistic continuum dynamics are, in Lagrangian form, *i.e.* along characteristics moving with the local material velocity $\vec{u}(\vec{r})$,

$$\frac{D\rho(\vec{r},t)}{Dt} = -\rho(\vec{r},t)\mathrm{div}\,\vec{u}(\vec{r},t) \tag{1}$$

$$\frac{D\vec{u}(\vec{r},t)}{Dt} = \frac{1}{\rho(\vec{r},t)}\mathrm{div}\,\tau(\vec{r},t) \tag{2}$$

$$\frac{De(\vec{r},t)}{Dt} = ||\tau(\vec{r},t)\mathrm{grad}\,\vec{u}(\vec{r},t)|| \tag{3}$$

where ρ is the mass density and e the specific internal energy. Changes in e can be related to changes in the temperature T through the heat capacity. The inherent properties of

3

each material in the problem are described by its constitutive relation or equation of state $\tau(s)$. As well as experiencing compression and work from mechanical deformation, the local material state $s(\vec{r}, t)$ can evolve through internal processes such as plastic flow. In general,

$$\frac{Ds(\vec{r},t)}{Dt} \equiv \dot{s}[s(\vec{r},t), U(\vec{r},t)] \quad : \quad U \equiv \text{grad}\,\vec{u}(\vec{r},t) \tag{4}$$

which can also include the equations for $\partial\rho/\partial t$ and $\partial e/\partial t$. Thus the material properties must describe at a minimum $\tau(s)$ and $\dot{s}[s(\vec{r},t), U(\vec{r},t)]$ for each material. If they also describe $T(s)$, the conductivity, and $\dot{s}(\dot{e})$, then heat conduction can be treated. Other functions may be needed for particular numerical methods in continuum dynamics, such as the need for wave speeds (e.g. the longitudinal sound speed), which are needed for time step control in explicit time integration. Internally, within the material properties models, it is desirable to re-use software as much as possible, and other functions of the state are therefore desirable to allow models to be constructed in a modular and hierarchical way. Arithmetic manipulations must be performed on the state during numerical integration, and these can be encoded neatly using operator overloading, so the operator of the appropriate type is invoked automatically without having to include 'if-then-else' structures for each operator as is the case in non-object-oriented programming languages such as Fortran-77. For instance, if $\dot{s}$ is calculated in a forward-time numerical method then changes of state are calculated using numerical evolution equations such as

$$s(t + \delta t) = s(t) + \delta t \dot{s}. \tag{5}$$

Thus for a general state s and its time derivative $\dot{s}$, which has an equivalent set of components, it is necessary to multiply a state by a real number and to add two states together. For a specific software implementation, other operations may be needed, for example to create, copy, or destroy a new instance of a state.

The attraction of this approach is that, by choosing a reasonably general form for the constitutive relation and associated operations, it is possible to separate the continuum dynamics part of the problem from the inherent behavior of the material. The relations describing the properties of different types of material can be encapsulated in a library form where the continuum dynamics program need know nothing about the relations for any specific type of material, and vice versa. The continuum dynamics programs and the material properties relations can be developed and maintained independently of each other, provided that the interface remains the same (Table I). This is an efficient way to make complicated

4

material models available for simulations of different types, including Lagrangian and Eulerian hydrocodes operating on different numbers of dimensions, and calculations of specific loading or heating histories such as shock and ramp loading discussed below. Software interfaces have been developed in the past for scalar EOS with a single structure for the state [12], but object-oriented techniques make it practical to extend the concept to much more complicated states, to combinations of models, and to alternative types of model selected when the program is run, without having to find a single super-set state encompassing all possible states as special cases.

A very wide range of types of material behavior can be represented with this formalism. At the highest level, different types of behavior are characterized by different structures for the state s (Table II). For each type of state, different specific models can be defined, such as perfect gas, polytropic and Grüneisen EOS. For each specific model, different materials are represented by choosing different values for the parameters in the model, and different local material states are represented through different values for the components of s. In the jargon of object-oriented programming, the ability to define an object whose precise type is undetermined until the program is run is known as polymorphism. For our application, polymorphism is used at several levels in the hierarchy of objects, from the overall type of a material (such as 'one represented by a pressure-density-energy EOS' or 'one represented by a deviatoric stress model') through the type of relation used to describe the properties of that material type (such as perfect gas, polytropic, or Grüneisen for a pressure-density-energy EOS, or Steinberg-Guinan [13] or Preston-Tonks-Wallace [14] for a deviatoric stress model), to the type of general mathematical function used to represent some of these relations (such as a polynomial or a tabular representation of $\gamma(\rho)$ in a polytropic EOS) (Table III). States or models may be defined by extending or combining other states or models – this can be implemented using the object-oriented programming concept of inheritance. Thus deviatoric stress models can be defined as an extension to *any* pressure-density-energy EOS (they are usually written assuming a specific type, such as Steinberg's cubic Grüneisen form), homogeneous mixtures can be defined as combinations of any pressure-density-temperature EOS, and heterogeneous mixtures can be defined as combinations of materials each represented by any type of material model.

Trial implementations have been made as libraries in the C++ and Java programming languages [15]. The external interface to the material properties was general at the level

of representing a generic material type and state. The type of state and model were then selected when programs using the material properties library were run. In C++, objects which were polymorphic at run time had to be represented as pointers, requiring additional software constructions to allocate and free up physical memory associated with each object. It was possible to include general re-usable functions as polymorphic objects when defining models: real functions of one real parameter could be polynomials, transcendentals, tabular with different interpolation schemes, piecewise definitions over different regions of the one dimensional line, sums, products, etc; again defined specifically at run time. Object-oriented polymorphism and inheritance were thus very powerful techniques for increasing software re-use, making the software more compact and more reliable through the greater use of functions which had already been tested.

Given conceptual and software structures designed to represent general material properties suitable for use in spatially-resolved continuum dynamics simulations, we now consider the use of these generic material models for calculating idealized loading paths.

III.   IDEALIZED ONE-DIMENSIONAL LOADING

Experiments to investigate the response of materials to dynamic loading, and to calibrate parameters in models of their behavior, are usually designed to apply as simple a loading history as is consistent with the transient state of interest. The simplest canonical types of loading history are shock and ramp [5, 6]. Methods of solution are presented for calculating the result of shock and ramp loading for materials described by generalized material models discussed in the previous section. Such direct solution removes the need to use a time- and space-resolved continuum dynamics simulation, allowing states to be calculated with far greater efficiency and without the need to consider and make allowance for attributes of resolved simulations such as the finite numerical resolution and the effect of numerical and artificial viscosities.

A.   Ramp compression

Ramp compression is taken here to mean compression or decompression. If the material is represented by an inviscid scalar EOS, *i.e.* ignoring dissipative processes and non-scalar

effects from elastic strain, ramp compression follows an isentrope. This is no longer true when dissipative processes such as plastic heating occur. The term 'quasi-isentropic' is sometimes used in this context, particularly for shockless compression; here we prefer to refer to the thermodynamic trajectories as adiabats since this is a more appropriate term: no heat is exchanged with the surroundings on the time scales of interest.

For adiabatic compression, the state evolves according to the second law of thermodynamics,

$$de = -p \, dv \tag{6}$$

i.e.

$$\dot{e} = -p \, \dot{v} = -\frac{p \mathrm{div}\vec{u}}{\rho}, \tag{7}$$

of for a more general material whose stress tensor is more complicated than a scalar pressure,

$$e = \tau_n \, dv \quad \Rightarrow \quad \dot{e} = \frac{\tau_n \mathrm{div}\vec{u}}{\rho} \tag{8}$$

where τ_n is the component of stress normal to the direction of deformation. The velocity gradient was expressed through a compression factor $\eta \equiv \rho'/\rho$ and a strain rate $\dot{\epsilon}$. In all ramp experiments used in the development and calibration of accurate material models, the strain has been applied uniaxially. More general strain paths, for instance isotropic or including a shear component, can be treated by the same formalism, and that the working rate is then a full inner product of the stress and strain tensors.

The acceleration or deceleration of the material normal to the wave as it is compressed or expanded adiabatically is

$$\frac{Du}{Dv} = -\sqrt{-\frac{\partial \tau_n}{\partial v}}, \tag{9}$$

from which it can be deduced that

$$\frac{Du}{D\rho} = \frac{c_l}{\rho} \tag{10}$$

where c_l is the longitudinal wave speed.

As with continuum dynamics, internal evolution of the material state can be calculated simultaneously with the continuum equations, or operator split and calculated periodically at constant compression [16]. The results are the same to second order in the compression increment. Operator-splitting is desirable when internal evolution can produce highly non-linear changes, such as reaction from solid to gas: rapid changes in state and properties can make numerical schemes unstable. Operator-splitting is also desirable when the integration

7

time step for internal evolution is much shorter than the continuum dynamics time step. Neither of these considerations is very important for ramp compression without spatial resolution, but operator-splitting was used as an option in the ramp compression calculations for consistency with continuum dynamics simulations.

The ramp compression equations were integrated using forward-time Runge-Kutta numerical schemes of second order. The fourth order scheme is a trivial extension. The sequence of operations to calculate an increment of ramp compression is as follows:

1. Time increment:
$$\delta t = -\frac{|\ln \eta|}{\dot{\epsilon}} \tag{11}$$

2. Predictor:
$$s(t + \delta t/2) = s(t) + \frac{\delta t}{2}\dot{s}_m(s(t), \dot{\epsilon}) \tag{12}$$

3. Corrector:
$$s(t + \delta t) = s(t) + \delta t \dot{s}_m(s(t + \delta t/2), \dot{\epsilon}) \tag{13}$$

4. Internal evolution:
$$s(t + \delta t) \rightarrow s(t + \delta t) + \int_t^{t+\delta t} \dot{s}_i(s(t'), \dot{\epsilon}) \, dt' \tag{14}$$

where $\dot{s}_m$ is the model-dependent state evolution from applied strain, and $\dot{s}_i$ is internal evolution at constant compression.

The independent variable for integration is specific volume v or mass density ρ; for numerical integration finite steps are taken in ρ and v. The step size $\Delta\rho$ can be controlled so that the numerical error during integration remains within chosen limits. A tabular adiabat can be calculated by integrating over a range of v or ρ, but when simulating experimental scenarios the upper limit for integration is usually that one of the other thermodynamic quantities reaches a certain value, for example that the normal component of stress reaches zero, which is the case on release from a high pressure state at a free surface. Specific end conditions were found by monitoring the quantity of interest until bracketed by a finite integration step, then bisecting until the stop condition was satisfied to a chosen accuracy. During bisection, each trial calculation was performed as an integration from the first side of the bracket by the trial compression.

B. Shock compression

Shock compression is the solution of a Riemann problem for the dynamics of a jump in compression moving with constant speed and with a constant thickness. The Rankine-Hugoniot (RH) equations [5] describing the shock compression of matter are derived in the continuum approximation, where the shock is a formal discontinuity in the continuum fields. In reality, matter is composed of atoms, and shocks have a finite width governed by the kinetics of dissipative processes – at a fundamental level, matter does not distinguish between shock compression and ramp compression with a high strain rate – but the RH equations apply as long as the width of the region of matter where unresolved processes occur is constant. Compared with the isentropic states induced by ramp compression in a material represented by an EOS, a shock always increases the entropy and hence the temperature. With dissipative processes included, the distinction between a ramp and a shock may become blurred.

The RH equations express the conservation of mass, momentum, and energy across a moving discontinuity in state. They are usually expressed in terms of the pressure, but are readily generalized for materials supporting shear stresses by using the component of stress normal to the shock (*i.e.*, parallel with the direction of propagation of the shock), τ_n:

$$u_s^2 = -v_0^2 \frac{\tau_n - \tau_{n0}}{v_0 - v}, \tag{15}$$

$$\Delta u_p = \sqrt{-(\tau_n - \tau_{n0})(v_0 - v)}, \tag{16}$$

$$e = e_0 - \frac{1}{2}(\tau_n + \tau_{n0})(v_0 - v), \tag{17}$$

where u_s is the speed of the shock wave with respect to the material, Δu_p is the change in material speed normal to the shock wave (*i.e.*, parallel to its direction of propagation), and subscript 0 refers to the initial state.

The RH relations can be applied to general material models if a time scale or strain rate is imposed, and an orientation chosen for the material with respect to the shock. Shock compression in continuum dynamics is almost always uniaxial.

The RH equations involve only the initial and final states in the material. If a material has properties that depend on the deformation path – such as plastic flow or viscosity – then physically the detailed shock structure may make a difference [17]. This is a limitation of discontinuous shocks in continuum dynamics: it may be addressed as discussed above

9

by including dissipative processes and considering ramp compression, if the dissipative processes can be represented adequately in the continuum approximation. Spatially-resolved simulations with numerical differentiation to obtain spatial derivatives and forward time differencing are usually not capable of representing shock discontinuities directly, and an artificial viscosity is used to smear shock compression over a few spatial cells [18]. The trajectory followed by the material in thermodynamic space is a smooth adiabat with dissipative heating supplied by the artificial viscosity. If plastic work is also included during this adiabatic compression, the overall heating for a given compression is greater than from the RH equations. To be consistent, plastic flow should be neglected while the artificial viscosity is non-zero. This localized disabling of physical processes, particularly time-dependent ones, during the passage of the unphysically smeared shock was previously found necessary for numerically stable simulations of detonation waves by reactive flow [19].

Detonation waves are reactive shock waves. Steady planar detonation (the Chapman-Jouguet state [20]) may be calculated using the RH relations, by imposing the condition that the material state behind the shock is fully reacted.

Several numerical methods have been used to solve the RH equations for materials represented by an EOS only [21, 22]. The general RH equations may be solved numerically for a given shock compression $\Delta\rho$ by varying the specific internal energy e until the normal stress from the material model equals that from the RH energy equation, Eq. 17. The shock and particle speeds are then calculated from Eqs 15 and 16. This numerical method is particularly convenient for EOS of the form $p(\rho, e)$, as e may be varied directly. Solutions may still be found for general material models using $\dot{s}(\dot{e})$, by which the energy may be varied until the solution is found.

Numerically, the solution was found by bracketing and bisection:

1. For given compression $\Delta\rho$, take the low-energy end for bracketing as a nearby state s_- (*e.g.* the previous state, of lower compression, on the Hugoniot), compressed adiabatically (to state $\tilde{s}$), and cooled so the specific internal energy is $e(s_-)$.

2. Bracket the desired state: apply successively larger heating increments Δe to $\tilde{s}$, evolving each trial state internally, until $\tau_n(s)$ from the material model exceeds $\tau_n(e - e_0)$ from Eq. 17.

3. Bisect in Δe, evolving each trial state internally, until $\tau_n(s)$ equals $\tau_n(e - e_0)$ to the

desired accuracy.

As with ramp compression, the independent variable for solution was mass density ρ, and finite steps $\Delta\rho$ were taken. Each shock state was calculated independently of the rest, so numerical errors did not accumulate along the shock Hugoniot. The accuracy of the solution was independent of $\Delta\rho$. A tabular Hugoniot can be calculated by solving over a range of ρ, but again when simulating experimental scenarios it is usually more useful to calculate the shock state where one of the other thermodynamic quantities reaches a certain value, often that u_p and τ_n match the values from another, simultaneous shock calculation for another material – the situation in impact and shock transmission problems, discussed below. Specific stop conditions were found by monitoring the quantity of interest until bracketed by a finite solution step, then bisecting until the stop condition was satisfied to a chosen accuracy. During bisection, each trial calculation was performed as a shock from the initial conditions to the trial shock compression.

C. Accuracy: application to air

The accuracy of these numerical schemes was tested by comparing with shock and ramp compression of a material represented by a perfect gas EOS,

$$p = (\gamma - 1)\rho e. \tag{18}$$

The numerical solution requires a value to be chosen for every parameter in the material model, here γ. Air was chosen as an example material, with $\gamma = 1.4$. Air at standard temperature and pressure has approximately $\rho = 10^{-3}\,\mathrm{g/cm^3}$ and $e = 0.25\,\mathrm{MJ/kg}$. Isentropes for the perfect gas EOS have the form

$$p\rho^{-\gamma} \quad \text{constant}, \tag{19}$$

and shock Hugoniots have the form

$$p = (\gamma - 1)\frac{2e_0\rho_0\rho + p_0(\rho - \rho_0)}{(\gamma + 1)\rho_0 - (\gamma - 1)\rho}. \tag{20}$$

The numerical solutions reproduced the principal isentrope and Hugoniot to $10^{-3}\%$ and 0.1% respectively, for a compression increment of 1% along the isentrope and a solution tolerance of $10^{-6}\,\mathrm{GPa}$ for each shock state (Fig. 1). Over most of the range, the error in the Hugoniot was 0.02% or less, only approaching 0.1% near the maximum shock compression.

IV. COMPLEX BEHAVIOR OF CONDENSED MATTER

The ability to calculate shock and ramp loci in state space, *i.e.* as a function of vary-ing loading conditions, is particularly convenient for investigating complex aspects of the response of condensed matter to dynamic loading. Each locus can be obtained by a single series of shock or ramp solutions, rather than having to perform a series of time- and space-resolved continuum dynamics simulations, varying the initial or boundary conditions and reducing the solution. We consider the calculation of temperature in the scalar EOS, the effect of material strength and the effect of phase changes.

A. Temperature

The continuum dynamics equations can be closed using a mechanical EOS relating stress to mass density, strain, and internal energy. Fo a scalar EOS, the ideal form to close the continuum equations is $p(\rho, e)$, with $s = \{\rho, e\}$ the natural choice for the primitive state fields. However, the temperature is needed as a parameter in physical descriptions of many contributions to the constitutive response, including plastic flow, phase transitions, and chemical reactions. Here, we discuss the calculation of temperature in different forms of the scalar EOS.

1. Density-temperature equations of state

If the scalar EOS is constructed from its underlying physical contributions for continuum dynamics, it may take the form $e(\rho, T)$, from which $p(\rho, T)$ can be calculated using the second law of thermodynamics [10]. An example is the 'SESAME' form of EOS, based on interpolated tabular relations for $\{p, e\}(\rho, T)$ [23]. A pair of relations $\{p, e\}(\rho, T)$ can be used as a mechanical EOS by eliminating T, which is equivalent to inverting $e(\rho, T)$ to find $T(\rho, e)$, then substituting in $p(\rho, T)$. For a general $e(\rho, T)$ relation, for example for the SESAME EOS, the inverse can be calculated numerically as required, along an isochore. In this way, a $\{p, e\}(\rho, T)$ can be used as a $p(\rho, e)$ EOS.

Alternatively, the same $p(\rho, T)$ relation can be used directly with a primitive state field including temperature instead of energy: $s = \{\rho, T\}$. The evolution of the state under mechanical work then involves the calculation of $\dot{T}(\dot{e})$, *i.e.* the reciprocal of the specific heat

capacity, which is a derivative of $e(\rho, T)$. As this calculation does not require $e(\rho, T)$ to be inverted, it is computationally more efficient to use $\{p, e\}(\rho, T)$ EOS with a temperature-based, rather than energy-based, state. The main disadvantage is that it is more difficult to ensure exact energy conservation as the continuum dynamics equations are integrated in time, but any departure from exact conservation is at the level of accuracy of the algorithm used to integrate the heat capacity.

Both structures of EOS have been implemented for material property calculations. Taking a SESAME type EOS, thermodynamic loci were calculated with $\{\rho, e\}$ or $\{\rho, T\}$ primitive states, for comparison (Fig. 2). For a monotonic EOS, the results were indistinguishable within differences from forward or reverse interpolation of the tabular relations. When the EOS, or the effective surface using a given order of interpolating function, was non-monotonic, the results varied greatly because of non-uniqueness when eliminating T for the $\{\rho, e\}$ primitive state.

2. Temperature model for mechanical equations of state

Mechanical EOS are often available as empirical, algebraic relations $p(\rho, e)$, derived from shock data. Temperature can be calculated without altering the mechanical EOS by adding a relation $T(\rho, e)$. While this relation could take any form in principle, one can also follow the logic of the Grüneisen EOS, in which the pressure is defined in terms of its deviation $\Delta p(\rho, e - e_r)$ from a reference curve $\{p_r, e_r\}(\rho)$. Thus temperatures can be calculated by reference to a compression curve along which the temperature and specific internal energy are known, $\{T_r, e_r\}(\rho)$, and a specific heat capacity defined as a function of density $c_v(\rho)$. In the calculations, this augmented EOS was represented as a 'mechanical-thermal' form comprising any $p(\rho, e)$ EOS plus the reference curves – an example of software inheritance and polymorphism.

One natural reference curve for temperature is the cold curve, $T_r = 0\,\mathrm{K}$. The cold curve can be estimated from the principal isentrope $e(\rho)|_{s_0}$ using the estimated density variation of the Grüneisen parameter:

$$e_r(\rho) = e(\rho)|_{s_0} - T_0 c_p e^{a(1 - \rho_0/\rho)} \left(\frac{\rho}{\rho_0} \right)^{\gamma_0 - a} \tag{21}$$

[24]. In this work, the principal isentrope was calculated in tabular form from the mechanical

EOS, using the ramp compression algorithm described above.

Empirical EOS are calibrated using experimental data. Shock and adiabatic compression measurements on strong materials inevitably include elastic-plastic contributions as well as the scalar EOS itself. If the elastic-plastic contributions are not taken into account self-consistently, the EOS may implicitly include contributions from the strength. A unique scalar EOS can be constructed to reproduce the normal stress as a function of compression for any unique loading path: shock or adiabat, for a constant or smoothly-varying strain rate. Such an EOS would not generally predict the response to other loading histories. The EOS and constitutive properties for the materials considered here were constructed self-consistently from shock data – this does not mean the models are accurate for other loading paths, as neither the EOS nor the strength model includes all the physical terms that real materials exhibit. This does not in any case matter for the purposes of demonstrating the properties of the numerical schemes.

This mechanical-thermal procedure was applied to Al using a Grüneisen EOS fitted to the same shock data used to calculate the $\{p, e\}(\rho, T)$ EOS discussed above [24]. Temperatures were in good agreement (Fig. 2). The mechanical-thermal calculations required a similar computational effort to the tabular $\{p, e\}(\rho, T)$ EOS with a $\{\rho, T\}$ primitive states (and were thus much more efficient than the tabular EOS with $\{\rho, e\}$ states), and described the EOS far more compactly.

B. Strength

For dynamic compressions to $o(10\,\mathrm{GPa})$ and above, on microsecond time scales, the flow stress of solids is often treated as a correction or small perturbation to the scalar EOS. However, the flow stress has been observed to be much higher on nanosecond time scales [25], and interactions between elastic and plastic waves may have a significant effect on the compression and wave propagation. The Rankine-Hugoniot equations should be solved self-consistently with strength included.

There is an inconsistency in the standard continuum dynamics treatment of scalar (pressure) and tensor (stress) response. The scalar EOS expresses the pressure $p(\rho, e)$ as the dependent quantity, which is the most convenient form for use in the continuum equations. Standard practice is to use sub-Hookean elasticity (hypoelastic form) [16] (Table II), in which the state parameters include the stress deviator σ, evolved by integration

$$\dot{\sigma} = G(s)\dot{\epsilon} \tag{22}$$

where G is the shear modulus and $\dot{\epsilon}$ the strain rate deviator. Thus the isotropic and deviatoric contributions to stress are not treated in an equivalent way: the pressure is calculated from a local state involving a strain-like parameter (mass density), whereas the stress deviator evolves with the time-derivative of strain. This inconsistency causes problems along complicated loading paths because G varies strongly with compression: if a material is subjected to a shear strain ϵ, then isotropic compression (increasing the shear modulus from G to G', leaving ϵ unchanged), then shear unloading to isotropic stress, the true unloading strain is $-\epsilon$, whereas the hypoelastic calculation would require a strain of $-\epsilon G/G'$. Using Be and the Steinberg-Guinan strength model as an example of the difference between hypoelastic and hyperelastic calculations, consider an initial strain to a flow stress of $0.3\,\mathrm{GPa}$ followed by isothermal, isotropic compression to $100\,\mathrm{GPa}$,. the strain to unload to a state of isotropic stress is 0.20% (hyperelastic) and 0.09% (hypoelastic). The discrepancy arises because the hypoelastic model does not increase the deviatoric stress under compression at constant deviatoric strain.

The stress can be considered as a direct response of the material to the instantaneous state of elastic strain: $\sigma(\epsilon, T)$. This relation can be predicted directly with electronic structure calculations of the stress tensor in a solid for a given compression and elastic strain state [11], and is a direct generalization of the scalar equation of state. A more consistent representation of the state parameters is to use the strain deviator ϵ rather than σ, and to calculate σ from scratch when required using

$$\sigma = G(s)\epsilon \tag{23}$$

– a hyperelastic formulation. The state parameters are then $\{\rho, e, \epsilon, \tilde{\epsilon}_p\}$.

The different formulations give different answers when deviatoric strain is accumulated

15

at different compressions, in which case the hyperelastic formulation is correct. If the shear modulus varies with strain deviator – *i.e.*, for nonlinear elasticity – then the definition of $G(\epsilon)$ must be adjusted to give the same stress for a given strain.

Many isotropic strength models use scalar measures of the strain and stress to parameterize work hardening and to apply a yield model of flow stress:

$$\tilde{\epsilon} = \sqrt{f_\epsilon ||\epsilon^2||}, \quad \tilde{\sigma} = \sqrt{f_\sigma ||\sigma^2||}. \tag{24}$$

Inconsistent conventions for equivalent scalar measures have been used by different workers. In the present work, the common shock physics convention was used that the flow stress component of τ_n is $\frac{2}{3}Y$ where Y is the flow stress. For consistency with published speeds and amplitudes for elastic waves, $f_\epsilon = f_\sigma = \frac{3}{2}$, in contrast to other values previously used for lower-rate deformation [26]. In principle, the values of f_ϵ and f_σ do not matter as long as the strength parameters were calibrated using the same values then used in any simulations.

2. Beryllium

The flow stress measured from laser-driven shock experiments on Be crystals a few tens of micrometers thick is, at around 5-9 GPa [25], much greater than the 0.3-1.3 GPa measured on microsecond time scales. A time-dependent crystal plasticity model for Be is being developed, and the behavior under dynamic loading depends on the detailed time dependence of plasticity. Calculations were performed with the Steinberg-Guinan strength model developed for microsecond scale data [24], and, for the purposes of rough comparison, with elastic-perfectly plastic response with a flow stress of 10 GPa. The elastic-perfectly plastic model neglected pressure- and work- hardening.

Calculations were made of the principal adiabat and shock Hugoniot, and of a release adiabat from a state on the principal Hugoniot. Calculations were made with and without strength. Considering the state trajectories in stress-volume space, it is interesting to note that heating from plastic flow may push the adiabat above the Hugoniot, because of the greater heating obtained by integrating along the adiabat compared with jumping from the initial to the final state on the Hugoniot (Fig. 3). Even with an elastic-perfectly plastic strength model, the with-strength curves do not lie exactly $\frac{2}{3}Y$ above the strengthless curves, because heating from plastic flow contributes an increasing amount of internal energy to the

EOS as compression increases.

An important characteristic for the seeding of instabilities by microstructural variations in shock response is the shock stress at which an elastic wave does not run ahead of the shock. In Be with the high flow stress of nanosecond response, the relation between shock and particle speeds is significantly different from the relation for low flow stress (Fig. 4). For low flow stress, the elastic wave travels at 13.2 km/s. A plastic shock travels faster than this for pressures greater than 110 GPa, independent of the constitutive model. The speed of a plastic shock following the initial elastic wave is similar to the low strength case, because the material is already at its flow stress, but the speed of a single plastic shock is appreciably higher.

For compression to a given normal stress, the temperature is significantly higher with plastic flow included. The additional heating is particularly striking on the principal adiabat: the temperature departs significantly from the principal isentrope. Thus ramp-wave compression of strong materials may lead to significant levels of heating, contrary to common assumptions of small temperature increases [27]. Plastic flow is largely irreversible, so heating occurs on unloading as well as loading. Thus, on adiabatic release from a shock-compressed state, additional heating occurs compared with the no-strength case. These levels of heating are important as shock or release melting may occur at a significantly lower shock pressure than would be expected ignoring the effect of strength. (Fig. 5.)

C. Phase changes

An important property of condensed matter is phase changes, including solid-solid polymorphism and solid-liquid. An equilibrium phase diagram can be represented as a single overall EOS surface as before. Multiple, competing phases with kinetics for each phase transformation can be represented conveniently using the structure described above for general material properties, for example by describing the local state as a set of volume fractions f_i of each possible simple-EOS phase, with transition rates and equilibration among them. This model is described in more detail elsewhere [19]. However, it is interesting to investigate the robustness of the numerical scheme for calculating shock Hugoniots when the EOS has the discontinuities in value and gradient associated with phase changes.

The EOS of molten metal, and the solid-liquid phase transition, can be represented to a

reasonable approximation as an adjustment to the EOS of the solid:

$$p_{\text{two-phase}}(\rho, e) = p_{\text{solid}}(\rho, \tilde{e}) \tag{25}$$

where

$$\tilde{e} = \begin{cases} e & : & T(\rho, e) < T_m(\rho) \\ e - \Delta \tilde{h}_m & : & \Delta \tilde{h}_m \equiv c_v(\rho, e)\left[T(\rho, e) - T_m(\rho)\right] < \Delta h_m \\ e - \Delta h_m & : & \text{otherwise} \end{cases} \tag{26}$$

and Δh_m is the specific latent heat of fusion. Taking the EOS and a modified Lindemann melting curve for Al [24], and using $\Delta h_m = 0.397\,\text{MJ/kg}$, the shock Hugoniot algorithm was found to operate stably across the phase transition (Fig. 6).

V. COMPOSITE LOADING PATHS

Given methods to calculate shock and adiabatic loading paths from arbitrary initial states, a considerable variety of experimental scenarios can be treated from the interaction of loading or unloading waves with interfaces between different materials, in planar geometry for uniaxial compression. The key physical constraint is that, if two dissimilar materials are to remain in contact after an interaction such as an impact or the passage of a shock, the normal stress τ_n and particle speed u_p in both materials must be equal on either side of the interface. The change in particle speed and stress normal to the waves were calculated above for compression waves running in the direction of increasing spatial ordinate (left to right). Across an interface, the sense is reversed for the material at the left. Thus a projectile impacting a stationary target to the right is decelerated from its initial speed by the shock induced by impact.

The general problem at an interface can be analyzed by considering the states at the instant of first contact – on impact, or when a shock traveling through a sandwich of materials first reaches the interface. The initial states are $\{u_l, s_l; u_r, s_r\}$. The final states are $\{u_j, s'_l; u_j, r'_r\}$ where u_j is the joint particle speed, $\tau_n(s'_l) = \tau_n(s'_r)$, and s'_i is connected to s_i by either a shock or an adiabat, starting at the appropriate initial velocity and stress, and with orientation given by the side of the system each material occurs on. Each type of wave is considered in turn, looking for an intersection in the $u_p - \tau_n$ plane. Examples of these wave interactions are the impact of a projectile with a stationary target (Fig. 7), release of a

shock state at a free surface or a material (*e.g.* a window) of lower shock impedance (hence reflecting a release wave into the shocked material – Fig. 8), reshocking at a surface with a material of higher shock impedance (Fig. 8), or tension induced as materials try to separate in opposite directions when joined by a bonded interface (Fig. 9). Each of these scenarios may occur in turn following the impact of a projectile with a target: if the target is layered then a shock is transmitted across each interface with a release or a reshock reflected back, depending on the materials; release ultimately occurs at the rear of the projectile and the far end of the target, and the oppositely-moving release waves subject the projectile and target to tensile stresses when they interact (Fig. 10).

As an illustration of combining shock and ramp loading calculations, consider the problem of an Al projectile, initially travelling at 3.6 km/s, impacting a stationary, composite target comprising a Mo sample and a LiF release window [28, 29]. The shock and release states were calculated using published material properties [24]. The initial shock state was calculated to have a normal stress of 63.9 GPa. On reaching the LiF, the shock was calculated to transmit at 27.1 GPa, reflecting as a release in the Mo. These stresses match the continuum dynamics simulation to within 0.1 GPa in the Mo and 0.3 GPa in the LiF, using the same material properties (Fig. 11). The associated wave and particle speeds match to a similar accuracy; wave speeds are much more difficult to extract from the continuum dynamics simulation.

An extension of this analysis can be used to calculate the interaction of oblique shocks with an interface [30].

VI.   CONCLUSIONS

A general formulation was developed to represent material models for applications in dynamic loading, suitable for software implementation in object-oriented programming languages. Numerical methods were devised to calculate the response of matter represented by the general material models to shock and ramp compression, and ramp decompression, by direct evaluation of the thermodynamic pathways for these compressions rather than spatially-resolved simulations. This approach is a generalization of earlier work on solutions for materials represented by a scalar equation of state. The numerical methods were found to be flexible and robust: capable of application to materials with very different properties. The numerical solutions matched analytic results to a high accuracy.

Care was needed with the interpretation of some types of physical response, such as plastic flow, when applied to deformation at high strain rates. The underlying time-dependence of processes occurring during deformation should be taken into account. The actual history of loading and heating experienced by material during the passage of a shock may influence the final state – this history is not captured in the continuum approximation to material dynamics, where shocks are treated as discontinuities. Thus care is also needed in spatially resolved simulations when shocks are modeled using artificial viscosity to smear them unphysically over a finite thickness.

Calculations were shown to demonstrate the operation of the algorithms for shock and ramp compression with material models representative of complex solids including strength and phase transformations.

The basic ramp and shock solution methods were coupled to solve for composite deformation paths, such as shock-induced impacts, and shock interactions with a planar interface between different materials. Such calculations capture much of the physics of typical material dynamics experiments, without requiring spatially-resolving simulations. The results of direct soliution of the relevant shock and ramp loading conditions were compared with hydrocode simulations, showing complete consistency.

---

[1] J.K. Dienes, J.M. Walsh, in R. Kinslow (Ed), "High-Velocity Impact Phenomena" (Academic Press, New York, 1970).

[2] D.J. Benson, Comp. Mech. **15**, 6, pp 558-571 (1995).

[3] J.W. Gehring, Jr, in R. Kinslow (Ed), "High-Velocity Impact Phenomena" (Academic Press, New York, 1970).

[4] R.M. Canup, E. Asphaug, Nature **412**, pp 708-712 (2001).

[5] For a recent review and introduction, see *e.g.* M.R. Boslough and J.R. Asay, in J.R. Asay, M. Shahinpoor (Eds), "High-Pressure Shock Compression of Solids" (Springer-Verlag, New York, 1992).

[6] For example, C.A. Hall, J.R. Asay, M.D. Knudson, W.A. Stygar, R.B. Spielman, T.D. Pointon, D.B. Reisman, A. Toor, and R.C. Cauble, Rev. Sci. Instrum. **72**, 3587 (2001).

[7] M.A. Meyers, "Dynamic Behavior of Materials" (Wiley, New York, 1994).

[8] G. McQueen, S.P. March, J.W. Taylor, J.N. Fritz, W.J. Carter, in R. Kinslow (Ed), "High-Velocity Impact Phenomena" (Academic Press, New York, 1970).

[9] J.D. Lindl, "Inertial Confinement Fusion" (Springer-Verlag, New York, 1998).

[10] D.C. Swift, G.J. Ackland, A. Hauer, G.A. Kyrala, Phys. Rev. B **64**, 214107 (2001).

[11] J.P. Poirier, G.D. Price, Phys. of the Earth and Planetary Interiors **110**, pp 147-56 (1999).

[12] I.N. Gray, P.C. Thompson, B.J. Parker, D.C. Swift, J.R. Maw, A. Giles and others (AWE Aldermaston), unpublished.

[13] D.J. Steinberg, S.G. Cochran, M.W. Guinan, J. Appl. Phys. **51**, 1498 (1980).

[14] D.L. Preston, D.L. Tonks, and D.C. Wallace, J. Appl. Phys. **93**, 211 (2003).

[15] Unsupported copies of the software may be obtained from the author, or commercially with support from Wessex Scientific and Technical Services Ltd, `www.wxres.com`

[16] D. Benson, Computer Methods in Appl. Mechanics and Eng. **99**, 235 (1992).

[17] J.L. Ding, J. Mech. and Phys. of Solids **54**, pp 237-265 (2006).

[18] J. von Neumann, R.D. Richtmyer, J. Appl. Phys. **21**, 3, pp 232-237 (1950).

[19] R.M. Mulford, D.C. Swift, in preparation.

[20] W. Fickett, W.C. Davis, "Detonation" (University of California Press, Berkeley, 1979).

[21] R. Menikoff, B.J. Plohr, Rev. Mod. Phys. **61**, pp 75-130 (1989).

[22] A. Majda, Mem. Amer. Math. Soc., **41**, 275 (1983).

[23] K.S. Holian (Ed.), *T-4 Handbook of Material Property Data Bases, Vol 1c: Equations of State*, Los Alamos National Laboratory report LA-10160-MS (1984).

[24] D.J. Steinberg, *Equation of State and Strength Properties of Selected Materials*, Lawrence Livermore National Laboratory report UCRL-MA-106439 change 1 (1996).

[25] D.C. Swift, T.E. Tierney, S.-N. Luo, D.L. Paisley, G.A. Kyrala, A. Hauer, S.R. Greenfield, A.C. Koskelo, K.J. McClellan, H.E. Lorenzana, D. Kalantar, B.A. Remington, P. Peralta, E. Loomis, Phys.Plasmas **12**, 056308 (2005).

[26] R. Hill, "The Mathematical Theory of Plasticity" (Clarendon Press, Oxford, 1950).

[27] C.A. Hall, Phys. Plasmas **7**, 5, pp 2069-2075 (2000).

[28] D.C. Swift, A. Seifter, D.B. Holtkamp, and D.A. Clark, Phys. Rev. B **76**, 054122 (2007).

[29] A. Seifter and D.C. Swift, Phys. Rev. B **77**, 134104 (2008).

[30] E. Loomis, D.C. Swift, J. Appl. Phys. **103**, 023518 (2008).

TABLE I: Interface to material models required for explicit forward-time continuum dynamics simulations.

purpose	interface calls
program set-up	read/write material data
continuum dynamics equations	stress(state)
time step control	sound speed(state)
evolution of state (deformation)	$d(\text{state})/dt(\text{state},\text{grad}\,\vec{u})$
evolution of state (heating)	$d(\text{state})/dt(\text{state},\dot{e})$
internal evolution of state	$d(\text{state})/dt$
manipulation of states	create and delete
	add states
	multiply state by a scalar
	check for self-consistency

Paremtheses in the interface calls denote functions, *e.g.* "stress(state)" for "stress as a function of the instantaneous, local state." The evolution functions are shown in the operator-split structure that is most robust for explicit, forward-time numerical solutions and can also be used for calculations of the shock Hugoniot and ramp compression. Checks for self-consistency include that mass density is positive, volume or mass fractions of components of a mixture add up to one, etc.

TABLE II: Examples of types of material model, distinguished by different structures in the state vector.

model	state vector s	effect of mechanical strain $\dot{s}_m(s, \mathrm{grad}u)$
mechanical equation of state	ρ, e	$-\rho\mathrm{div}\vec{u}, -p\mathrm{div}\vec{u}/\rho$
thermal equation of state	ρ, T	$-\rho\mathrm{div}\vec{u}, -p\mathrm{div}\vec{u}/\rho c_v$
heterogeneous mixture	$\{\rho, e, f_v\}_i$	$\{-\rho\mathrm{div}\vec{u}, -p\mathrm{div}\vec{u}/\rho, 0\}_i$
homogeneous mixture	$\rho, T, \{f_m\}_i$	$\{-\rho\mathrm{div}\vec{u}, -p\mathrm{div}\vec{u}/\rho c_v, 0_i$
traditional deviatoric strength	$\rho, e, \sigma, \tilde{\epsilon}_p$	$-\rho\mathrm{div}\vec{u}, \frac{-p\mathrm{div}\vec{u}+f_p\|\sigma\dot{\epsilon}_p\|}{\rho}, G\dot{\epsilon}_e,$ $\sqrt{f_\epsilon\|\dot{\epsilon}_p^2\|}$

The symbols are ρ: mass density; e: specific internal energy, T: temperature, f_v: volume fraction, f_m: mass fraction, σ: stress deviator, f_p: fraction of plastic work converted to heat, $\mathrm{grad}u_p$: plastic part of velocity gradient, G: shear modulus, $\dot{\epsilon}_{e,p}$: elastic and plastic parts of strain rate deviator, $\tilde{\epsilon}_p$: scalar equivalent plastic strain, f_ϵ: factor in effective strain magnitude. Reacting solid explosives can be represented as heterogeneous mixtures, one component being the reacted products; reaction, a process of internal evolution, transfers material from unreacted to reacted components. Gas-phase reaction can be represented as a homogeneous mixture, reactions transferring mass between components representing different types of molecule. Symmetric tensors such as the stress deviator are represented more compactly by their 6 unique upper triangular components, *e.g.* using Voigt notation.

TABLE III: Outline hierarchy of material models, illustrating the use of polymorphism (in the object-oriented programming sense).

material (or state) type	model type
mechanical equation of state	polytropic, Grüneisen, energy-based Jones-Wilkins-Lee, (ρ, T) table, etc
thermal equation of state	temperature-based Jones-Wilkins-Lee, quasiharmonic, (ρ, T) table, etc
reactive equation of state	modified polytropic, reactive Jones-Wilkins-Lee
spall	Cochran-Banner
deviatoric stress	elastic-plastic, Steinberg-Guinan, Steinberg-Lund, Preston-Tonks-Wallace, etc
homogeneous mixture	mixing and reaction models
heterogeneous mixture	equilibration and reaction models

Continuum dynamics programs can refer to material properties as an abstract 'material type' with an abstract material state. The actual type of a material (*e.g.* mechanical equation of state), the specific model type (*e.g.* polytropic), and the state of material of that type are all handled transparently by the object-oriented software structure.

The reactive equation of state has an additional state parameter λ, but and the software operations are defined by extending those of the mechanical equation of state. Spalling materials can be represented by a solid state plus a void fraction f_v, with operations defined by extending those of the solid material. Homogeneous mixtures are defined as a set of thermal equations of state, and the state is the set of states and mass fractions for each. Heterogeneous mixtures are defined as a set of 'pure' material properties of any type, and the state is the set of states for each component plus its volume fraction.
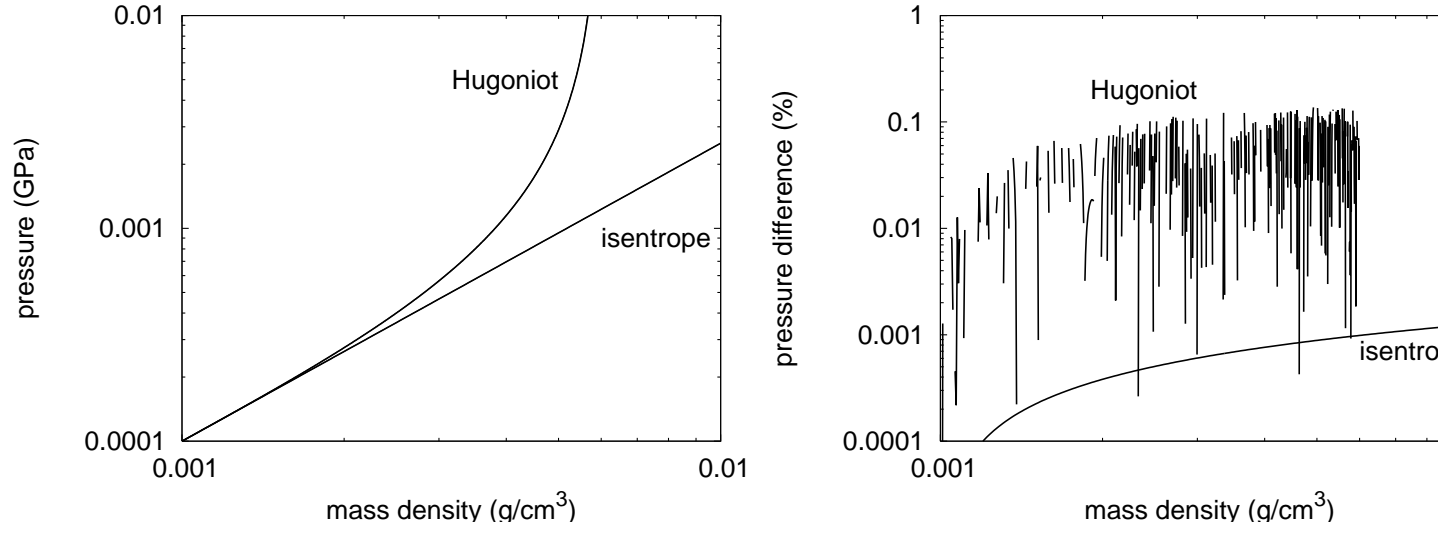
FIG. 1: Principal isentrope and shock Hugoniot for air (perfect gas): numerical calculations for general material models, compared with analytic solutions.
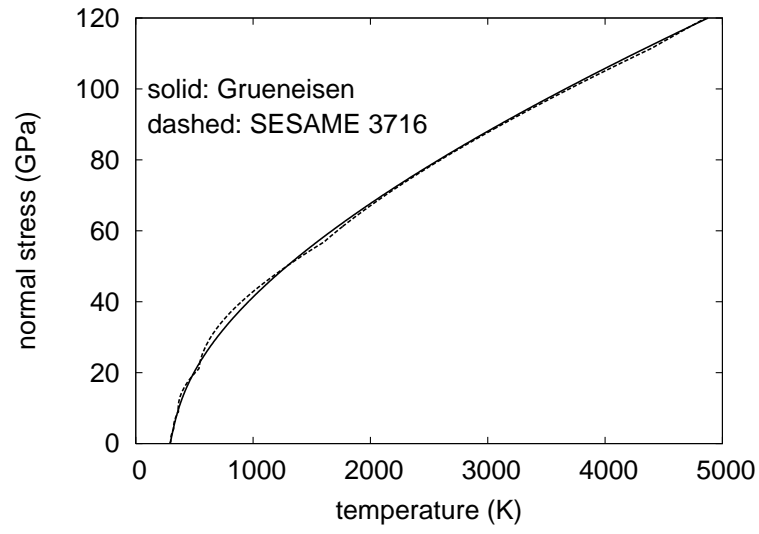
FIG. 2: Shock Hugoniot for Al in pressure-temperature space, for different representations of the equation of state.
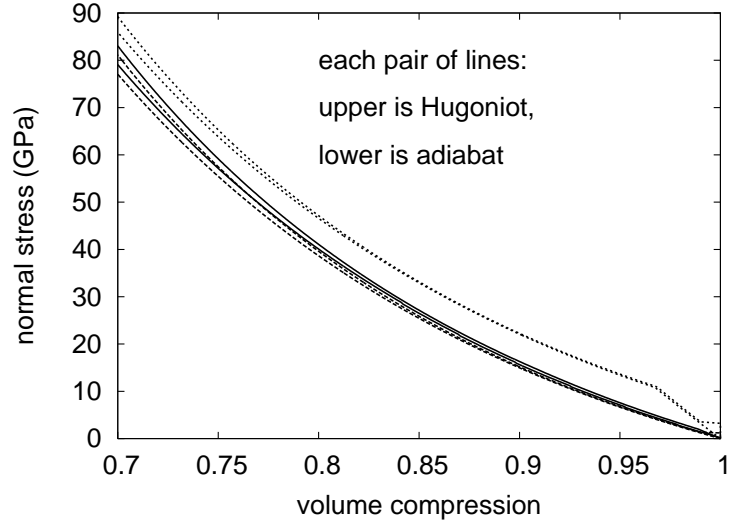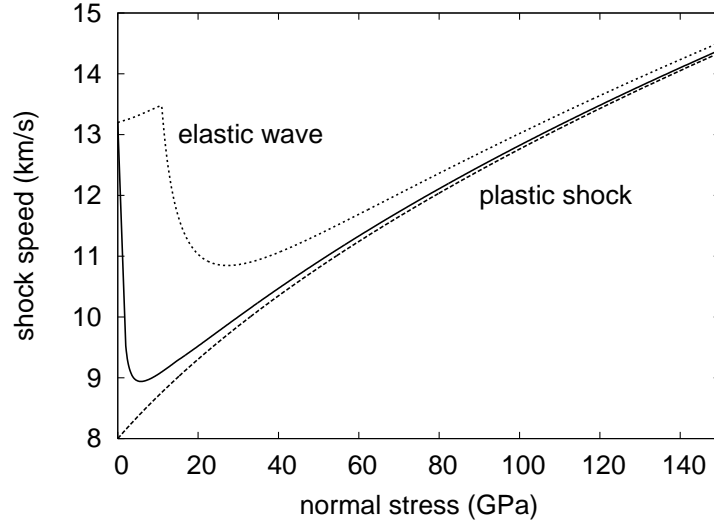
FIG. 3: Principal adiabat and shock Hugoniot for Be in normal stress-compression space, neglecting strength (dashed), for Steinberg-Guinan strength (solid), and for elastic-perfectly plastic with $Y = 10\,\mathrm{GPa}$ (dotted).
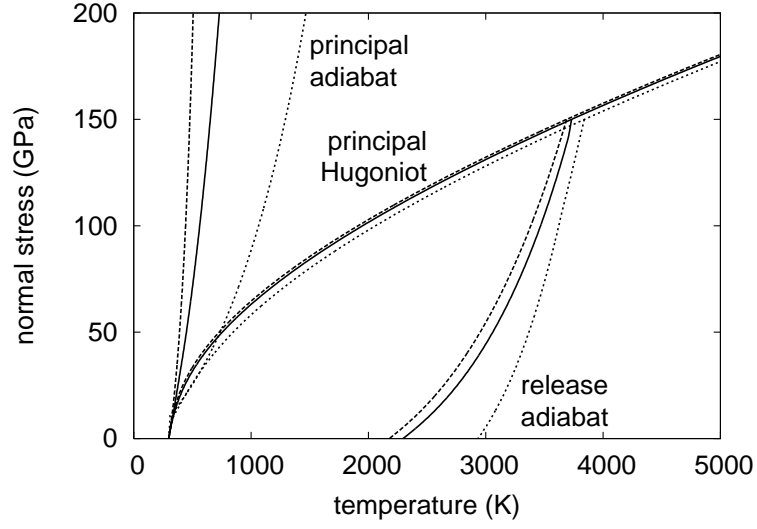
FIG. 4: Principal adiabat and shock Hugoniot for Be in shock speed-normal stress space, neglecting strength (dashed), for Steinberg-Guinan strength (solid), and for elastic-perfectly plastic with $Y = 10\,\text{GPa}$ (dotted).

FIG. 5: Principal adiabat, shock Hugoniot, and release adiabat for Be in normal stress-temperature space, neglecting strength (dashed), for Steinberg-Guinan strength (solid), and for elastic-perfectly plastic with $Y = 10\,\text{GPa}$ (dotted).
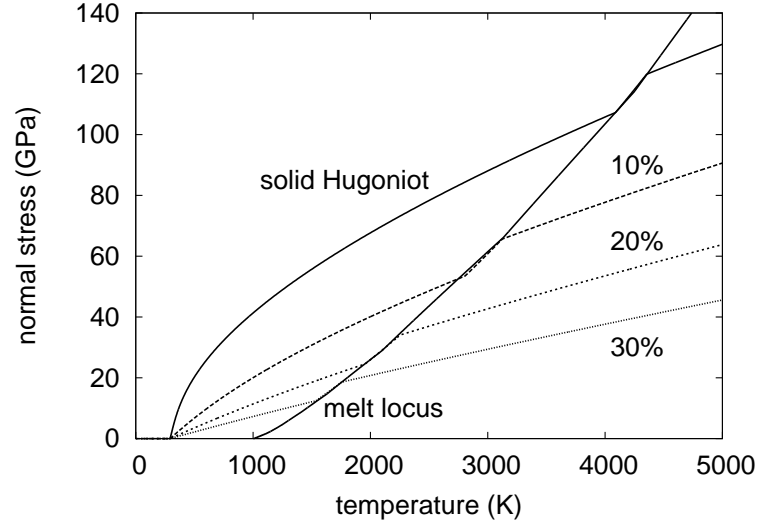
FIG. 6: Demonstration of shock Hugoniot solution across a phase boundary: shock-melting of Al, for different initial porosities.
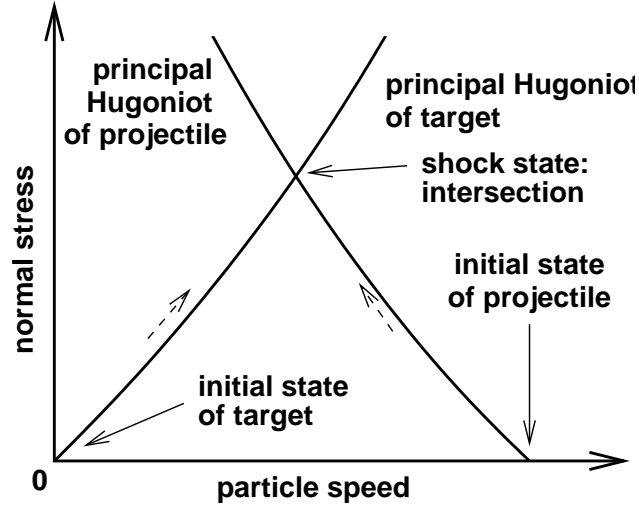
FIG. 7: Wave interactions for the impact of a flat projectile moving from left to right with a stationary target. Dashed arrows are a guide to the sequence of states. For a projectile moving from right to left, the construction is the mirror image reflected in the normal stress axis.
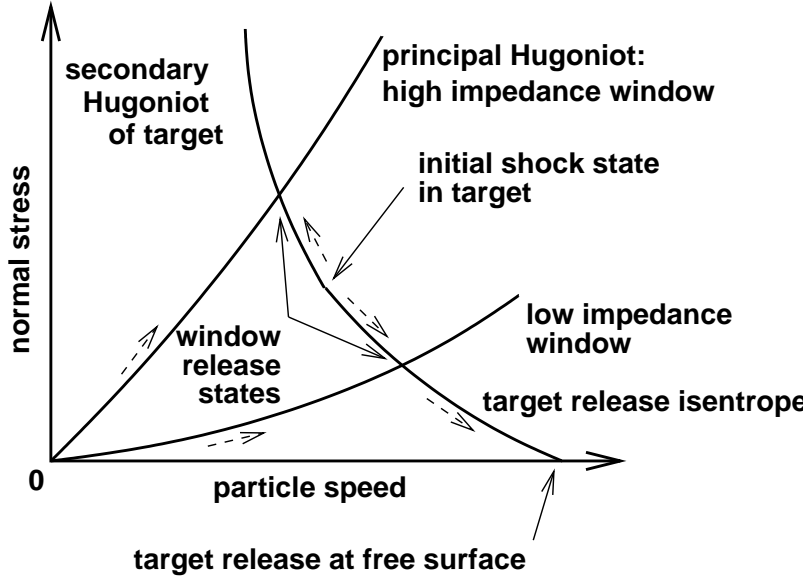
FIG. 8: Wave interactions for the release of a shocked state (shock moving from left to right) into a stationary 'window' material to its right. The release state depends whether the window has a higher or lower shock impedance than the shocked material. Dashed arrows are a guide to the sequence of states. For a shock moving from right to left, the construction is the mirror image reflected in the normal stress axis.
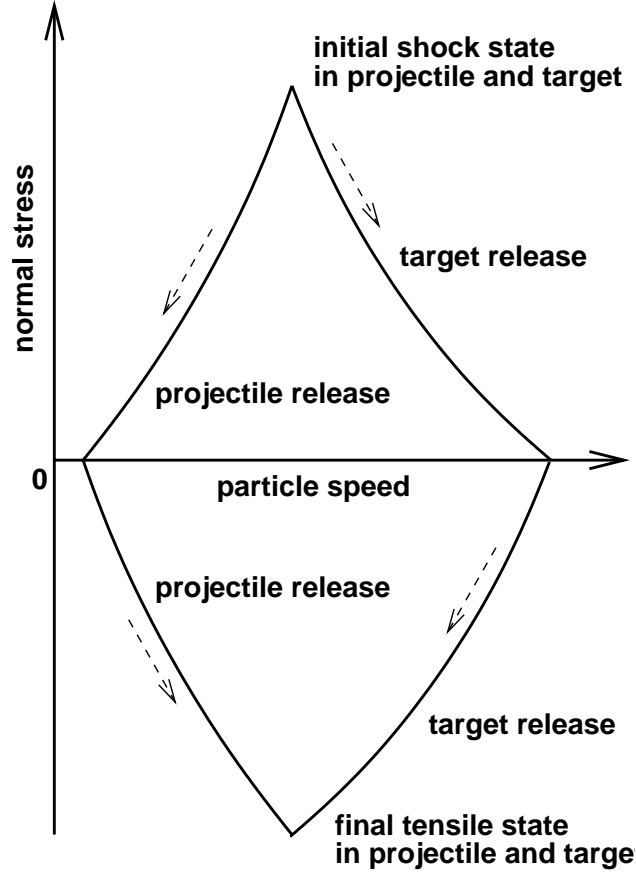
FIG. 9: Wave interactions for the release of a shocked state by tension induced as materials try to separate in opposite directions when joined by a bonded interface. Material damage, spall, and separation are neglected: the construction shows the maximum tensile stress possible. For general material properties, *e.g.* if plastic flow is included, the state of maximum tensile stress is not just the negative of the initial shock state. Dashed arrows are a guide to the sequence of states. The graph shows the initial state after an impact by a projectile moving from right to left; for a shock moving from right to left, the construction is the mirror image reflected in the normal stress axis.
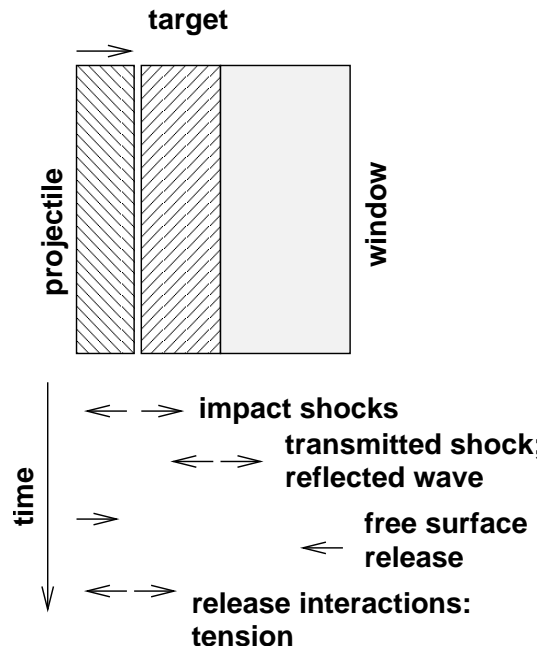
FIG. 10: Schematic of uniaxial wave interactions induced by the impact of a flat projectile with a composite target.
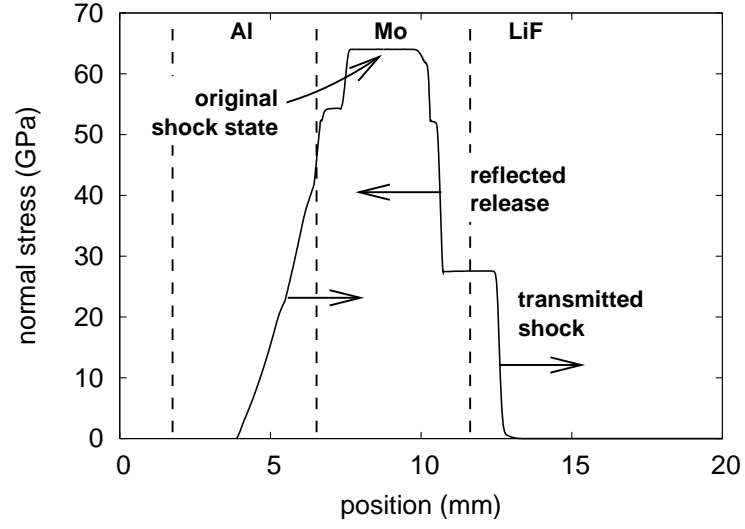
FIG. 11: Hydrocode simulation of Al projectile at 3.6 km/s impacting a Mo target with a LiF release window, 1.1 μs after impact. Structures on the waves are elastic precursors.